Available online at www.sciencedirect.com
ScienceDirect
Journal of the European Ceramic Society 30 (2010) 1879–1885
www.elsevier.com/locate/jeurceramsoc

Build-up formation and corrosion of monolithic refractories in cement kiln preheaters

I. Recio Dominguez [a], J. Gómez-Millán [b], M. Alvarez [b], S. De Aza [c], L. Contreras [c], A.H. De Aza [c,*]

[a] *Refractarios ALFRAN México S.A. de C.V., Nuevo León, Mexico*
[b] *Refractarios ALFRAN S.A., Sevilla, Spain*
[c] *Instituto de Cerámica y Vidrio (CSIC), C/Kelsen 5, Madrid, Spain*

Received 24 August 2009; received in revised form 8 February 2010; accepted 27 February 2010
Available online 2 April 2010

Abstract

Nowadays, the cost of energy and the environmental standards have encouraged cement manufacturers to replace conventional fuels by alternative fuels (industrial wastes and agricultural and forest residues). Therefore, the increasing uses of these alternative fuels in cement plants have severely increased build-up formation and attack of the monolithic refractories used. All this strongly affects the durability of the refractory castables. In order to investigate this issue a number of samples, taken from five cement kiln preheaters, were studied. The results obtained confirm that the build-up constitution varies broadly and they consist of alternate layers of slightly different compositions as a consequence of changes in operating conditions of the furnaces. Their growth and compactness are due to a vitreous phase formation. On the other hand, the main compounds causing the attack of the monolithic refractories are: K_2O, SO_3, CaO and Cl^-. These give place, in the matrix of the refractory material, to a liquid phase together with minor amounts of different crystalline phases. The depth of the attack depends on the SiC content in the refractory castable, as the proportion of SiC in the matrix increases the depth of attack decreases. The liquid phase brings about the adherence of the ring to the refractory castables. Therefore, when build-up is removed, part of the refractory material adhered to them is also removed. The thickness of the peeled off material depends on the depth of the attack.

Keywords: Refractories; Corrosion; Cement kilns; Build-up; SiC

1. Introduction

In cement production plants the use of monolithic refractories has seen gradual increase in the preheater, inlet and outlet kilns and coolers. Improvement in density and strength of the low cement castables has greatly contributed to this trend. Their installation method: poured castables (with vibration casting), gunning materials and wet gunning materials (shotcreting), vary depending on the requirement of the region of the furnace where they are applied (high abrasion resistance, decrease adherence of the cement clinker, etc.).[1,2]

In the preheater zone, fireclay castables with different percentages of SiC up to 50 wt.% have been recommended[3] and successfully used.[4] However, nowadays, costs energy and environmental standards have encouraged cement manufacturers to replace conventional fuels by alternative fuels (industrial wastes and agricultural and forest residues).[5–9] As a result, build-up formation[10,11] and the attack of the monolithic refractories have greatly increased.[12,13]

In order to investigate this, and to establish the formation mechanism of kiln rings and their subsequent build-ups, as well as the attack and destruction of the refractory castables, a number of samples taken from five cement kiln preheaters have been studied.

Table 1 shows the conventional and alternative fuels employed and their use into the main burner or into the calciner burner for the five cement kilns studied.

2. Experimental procedure

2.1. Samples

These were taken by diamond drilling from different areas (Fig. 1) of the preheaters of five cement kilns. All the samples were studied by the following methods.

* Corresponding author. Tel.: +34 91 7355864; fax: +34 91 7355843.
E-mail address: aaza@icv.csic.es (A.H. De Aza).
URL: http://www.alfran.es/ (A.H. De Aza).

0955-2219/$ – see front matter © 2010 Elsevier Ltd. All rights reserved.
doi:10.1016/j.jeurceramsoc.2010.02.023

Table 1
Conventional and alternative fuels employed and their use into the main burner or into the calciner burner for the cement kilns studied.

Fuels	Rotary kiln I			Rotary kiln II			Rotary kiln III			Rotary kiln IV			Rotary kiln V		
	%	Main burner	2nd burner	%	Main burner	2nd burner	%	Main burner	2nd burner	%	Main burner	2nd burner	%	Main burner	2nd burner
Petroleum coke	96	88	12	83	80	20	88	75	10	87	50	50	94	94	–
Fuel oil	0.27	↓	–	3	↓	–	–	–	–	0.4	↓	–	2	↓	–
Rice husk	1.74	↓+	↓+	–	–	–	–	–	–	–	–	–	–	–	–
Residues of forest pruning	0.99	–	↓+	–	–	–	–	–	–	–	–	–	4	↓+	–
Olive waste	0.33	↓+	↓+	–	–	–	–	–	–	–	–	–	–	–	–
Bituminous coal	0.67	↓+	↓+	–	–	–	–	–	–	–	–	–	–	–	–
Meat meal	–	–	–	13	↓+	–	5	↓+	↓+	4.6	↓+	–	–	–	–
Liquid waste	–	–	–	3	↓+	–	–	–	–	–	–	–	–	–	–
Heavy fuel oil	–	–	–	–	–	–	3	↓+	↓+	–	–	–	–	–	–
Sliced tires	–	–	–	–	–	–	2	–	↓+	3.3	–	↓+	–	–	–
Plastic waste	–	–	–	–	–	–	2	↓+	–	–	–	–	–	–	–
Sewage sludge	–	–	–	–	–	–	–	–	–	3.7	↓+	–	–	–	–

2nd burner = calciner burner; ↓ = used only at the beginning of the process; ↓+ = blended with the coke in the mills.

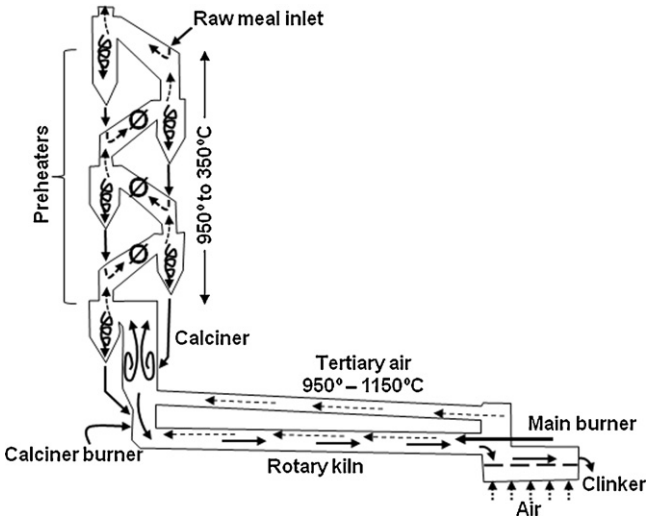

Fig. 1. Graphical scheme of a cement kiln showing the locations (Ø) from which the samples were taken.

2.2. Chemical analysis

The chemical analysis was performed in all cases in a MagiX Super Q Version 3.0 X-ray fluorescence spectrometer (Philips, The Netherlands) provided with an Rh X-ray tube and a power generator of 2.4 kW. Powdered samples weighing 0.3000 g were mixed with 5.5 g of spectral grade $Li_2B_4O_7$ and melted in a Pt/Au crucible and shaped into glass disks in a special controlled furnace Perl'X3 (Philips, The Netherlands). Calibration curves were prepared from standards of certified composition of natural and appropriated synthetic compounds. The carbon and the sulphur were determined by LECO. The concentrations of chlorine, bromine and impurities which are not detected in the analysis of the glass disk were determined by analysis on pressed pellets of the powdered samples. The analysis of the alkalis was determined by flame photometry. Finally, losses of ignition were calculated from the thermogravimetric data of the samples.

2.3. X-ray diffraction

To evaluate the phase's composition, X-ray diffraction (XRD) patterns were obtained in a Kristalloflex D5000 diffractometer provided with a generator Kristalloflex 710 (Siemens, Germany). Anode voltage and current were 40 kV and 30 mA, respectively. Bragg–Brentano geometry and monochrome (secondary graphite monochromator) Cu $K_{\alpha 1,2}$ radiation ($\lambda = 1.5418$ Å) were employed. The interval 2–70° (2θ) was scanned with a step size of 0.05° and time/step of 1.5 s. Measurements were done on powdered samples rotating at a frequency of 0.5 s^{-1}. Diffractograms of samples were compared to data provided by the Joint Committee on Powder Diffraction Standards (JCPDS) database.

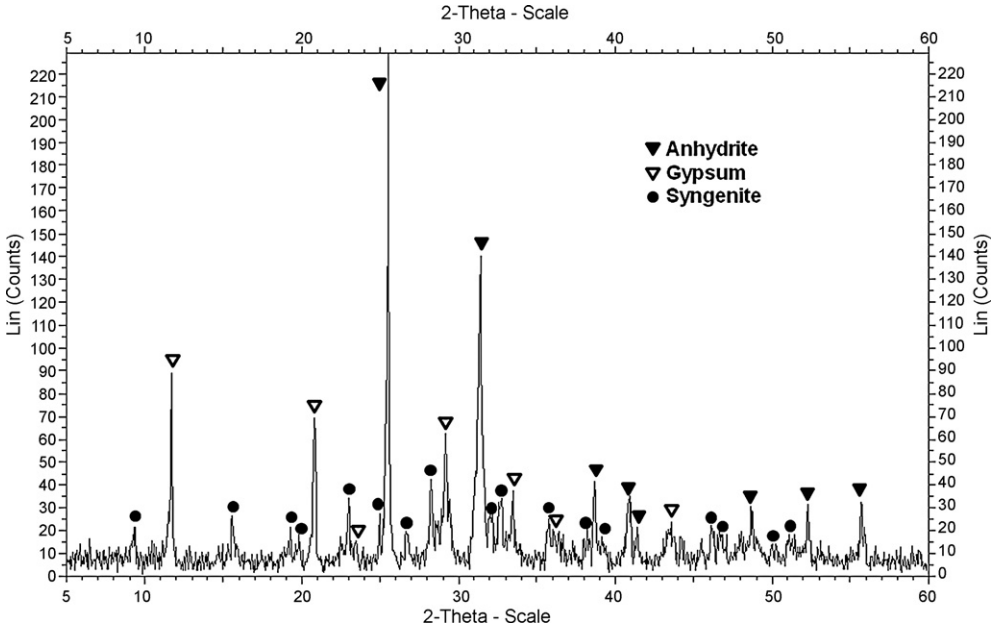

Fig. 2. Typical X-ray diffraction of a build-up where anhydrite is the predominant phase together with gypsum and syngenite in minor amounts.

2.4. Thermal analysis

Differential thermal (DTA) and thermogravimetric (TGA) analyses were performed in a simultaneous thermoanalysis apparatus STA 409 CD (NETZSCH-Gerätebau GmbH, Selb, Germany) at a heating rate of 5 °C/min up to 1300 °C in air, using Pt crucibles and α-Al_2O_3 as reference.

Table 2
Variation range of the main constituents in wt.%.

SO_3	13.3–42.56
CaO	36.46–57.84
K_2O	3.49–8.98
Cl^-	0.51–4.44

2.5. Microstructural study

The microstructure of polished samples was studied by means of Optical (RLM) and Scanning Electron Microscopies (SEM). A Reflected-Light Optical Microscope, model HP1 (Karl Zeiss, Oberköchen & Jena, Germany), and a Field Emission Scanning Electron Microscope, model S-4700 (Hitachi High-Technologies Corp., Tokyo, Japan), were used. The chem-

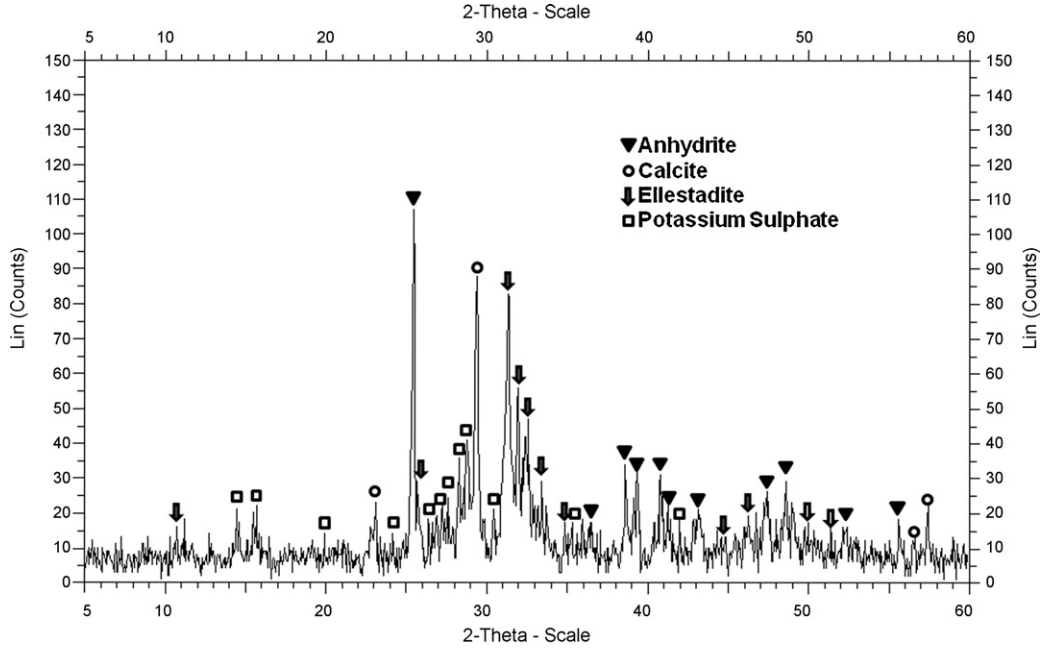

Fig. 3. Typical X-ray diffraction of a build-up where anhydrite, calcite and ellestadite are the predominant phases together with minor amounts of potassium sulphate.

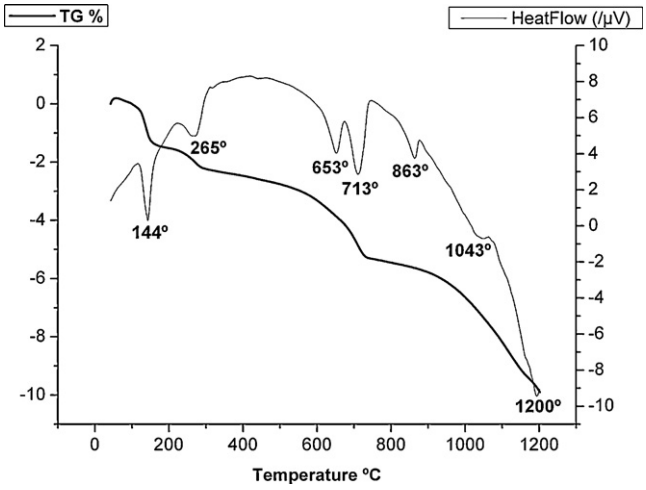

Fig. 4. DTA/TG of one of the build-up studied.

ical composition of crystalline grains and vitreous phase at the matrixes was semi-quantitatively determined with an Energy Dispersive X-Ray Spectrometer (EDS) system, coupled to the above described electron microscope.

3. Results and discussion

3.1. Build-up

The chemical analysis of the build-up samples has shown that the main constituents: SO_3, K_2O, CaO and Cl^-, vary their proportions between broad limits as shown in Table 2.

On the other hand, X-ray diffractions have shown that anhydrite ($CaSO_4$) (Fig. 2) or a mixture of anhydrite and calcite ($CaCO_3$) (Fig. 3) is normally the predominant phases in most of the samples studies. Less amounts of other phases such as: ellestadite[14] solid solution ($Ca_{10}(SiO_4)_3(SO_4)_3Z_2$) ($Z$ = OH, F, Cl), more frequently chlorellestadite[15–17] ($Ca_{10}(SiO_4)_3(SO_4)_3Cl_2$) and spurrite ($Ca_5(SiO_4)_2CO_3$)[18] have also been determined often. Finally, minor amounts of syngenite ($K_2Ca(SO_4)_2(H_2O)$)[19] and even gypsum ($CaSO_4{\cdot}2H_2O$) were also present in some samples. The last phase, formed during the cooling of the furnace, was mainly confirmed by DTA/TG. Fig. 4 shows a typical DTA/TG of the build-up studied. As it can be seen, there are two endothermic effects between room temperature and 300 °C, attributed to dehydration of gypsum, whose percentage by weight, according to the TG, is approximately 12.9%. Subsequently, there are two endothermic effects, at 653 °C and 713 °C, attributed to the sylvite ($K_{1-x}Na_xCl$) melting and the $CaCO_3$ decomposition. Lastly, there are three endothermic effects at 863 °C, 1043 °C and 1200 °C, with a weight loss associated with them, of about 4.39%. These are attributed to the chlorellestadite decomposition with $CaCl_2$ volatilization and transformation into ternesite[20] ($Ca_5(SiO_4)_2(SO_4)$), anhydrite ($CaSO_4$) and Ca_2SiO_4. Ternesite subsequently transforms into anhydrite and more dicalcium silicate (Ca_2SiO_4) and, finally, anhydrite melts. The sequence of the reaction is as follows:

$$Ca_{10}(SiO_4)_3(SO_4)_3CaCl_2 \rightarrow CaCl_2{\uparrow} + Ca_5(SiO_4)_2(SO_4) + 2(CaSiO_4) + Ca_2SiO_4, \quad (1)$$

$$Ca_5(SiO_4)_2(SO_4) \rightarrow CaSO_4 + 2(Ca_2SiO_4). \quad (2)$$

Microstructural examination of the samples of the build-up, by RLM and SEM-EDS, showed that the growth-up of the rings is due to successive deposition of the phases previously mentioned. Their morphology, as it is shown in Fig. 5, consists of alternate layers with slight variations in composition as a result of changes in operating conditions of the furnaces. SEM-EDS cross-section, of sample of Fig. 5, shows clearly the banded morphology (Fig. 6) and Table 3 shows the analytical variation between them. As shown in the table, SO_3, CaO and K_2O are the main components. However, the presence of Cl^-, even in small

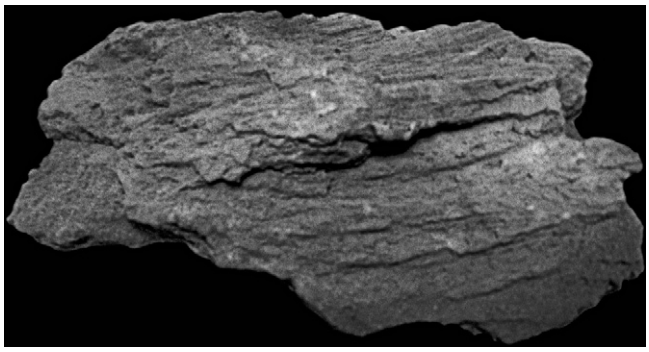

Fig. 5. Photograph showing the layered structure of a build-up.

Table 3
EDS, semi-quantitative chemical analysis of the areas marked in Fig. 6.

	Na_2O	MgO	Al_2O_3	SiO_2	SO_3	Cl^-	K_2O	CaO
pt1	0.17	0.56	0.30	1.73	52.01	1.53	3.86	38.84
pt2	0.00	0.00	0.04	1.12	43.68	2.58	24.03	27.57
pt3	0.10	0.13	0.47	1.17	51.61	1.76	30.13	14.64

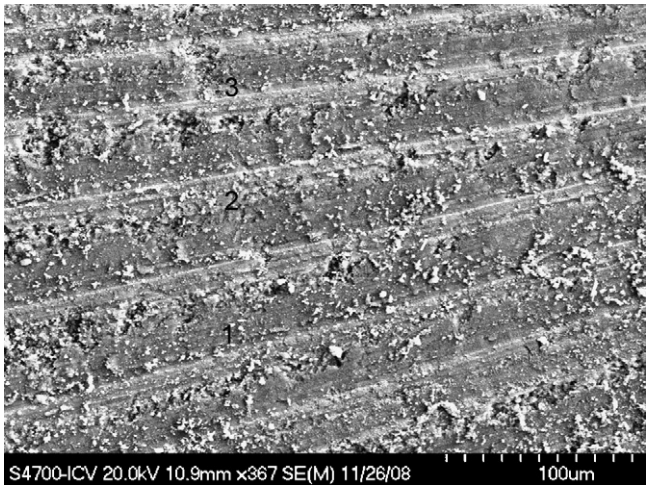

Fig. 6. SEM micrograph, of the cross-section of Fig. 4, showing the areas analyzed.

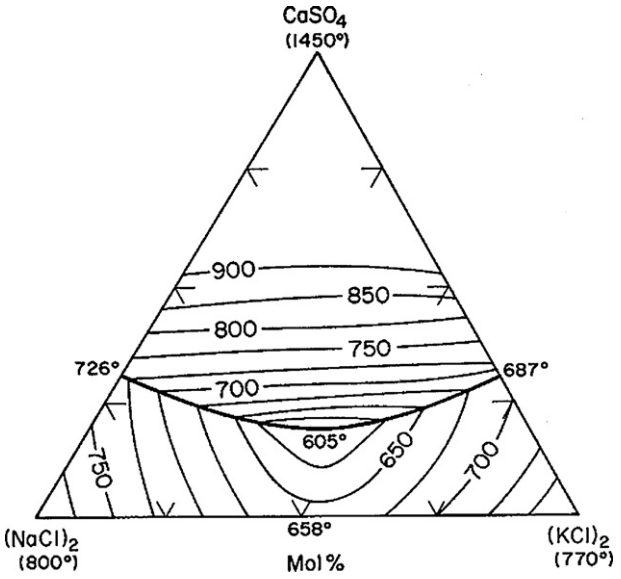

Fig. 7. The KCl–NaCl–$CaSO_4$ ternary system.[21]

quantities, is the main cause of the formation of a glassy phase at very low temperature, as shown in Fig. 7. As it can be seen, the system KCl–NaCl–$CaSO_4$[21] shows that sylvite ($K_{1-x}Na_xCl$), a solid solution between potassium chloride (KCl) and sodium chloride (NaCl), has a melting point at 658 °C, that in the presence of anhydrite ($CaSO_4$), gives place to a minimum invariant point at 605 °C. The vitreous phase, formed at this temperature, is the main cause of build-up formation and their subsequent build-ups and also of their compactness.

3.2. Monolithic refractories

The study of the monolithic refractories was carried out giving special attention to the refractory castable/build-up interface. A first RLM observation showed that the depth of attack in the refractory castable varies greatly, from a few millimeters to several centimeters, depending on the SiC content in the samples: the higher the SiC content the lower the impregnation.

Table 4
Minimum and maximum analytical values of the main corrosion agents in wt.%.

K_2O	2.20–9.03
SO_3	0.33–7.50
CaO	2.62–7.42
Cl^-	0.15–2.91

Table 4 shows minimum and maximum analytical values, determined in the different samples studied, of the compounds considered responsible for the attack, taking away the principal components of the refractory castables, such as Al_2O_3, SiO_2, SiC, etc. The analytical results showed that the main compounds, causing the attack of the monolithic refractories, are: K_2O, SO_3, CaO and Cl^-, in this order. Their percentages vary broadly, as previously in build-up, depending on the operating conditions of the kilns and also of the proportions in the use of traditional and alternative fuels. In Table 4, the CaO content has to be decreased in ~2 wt.%, the normal average value of CaO in the refractory castables studied.

Studies by X-ray diffraction showed, besides the presence of the main constituents of the refractory castables: mullite ($Al_6Si_2O_{13}$), corundum (Al_2O_3) and silicon carbide (SiC), and in some cases, quartz (α-SiO_2) and cristobalite (α-SiO_2), the presence of the following phases: feldspar type ($K_{1-x}Na_xAlSi_3O_8$), chloresllestadite ($Ca_{10}(SiO_4)_3(SO_4)_3CaCl_2$) and in some cases potassium calcium sulphate type ($K_2Ca_{2-x}(SO_4)_{3-x}$) and even sylvite ($K_{1-x}Na_xCl$) and ternesite ($Ca_5(SiO_4)_2(SO_4)_2$), all these phases in very small amounts. In those samples with less SiC content (~5 wt.%), where the depth of attack was greater, a higher percentage of feldspar (Leucite) was detected (Fig. 8). The formation of this phase gives place to a big volume expansion (~20%), which contributes to increase the permeability of the refractory castable as well as its weakness.

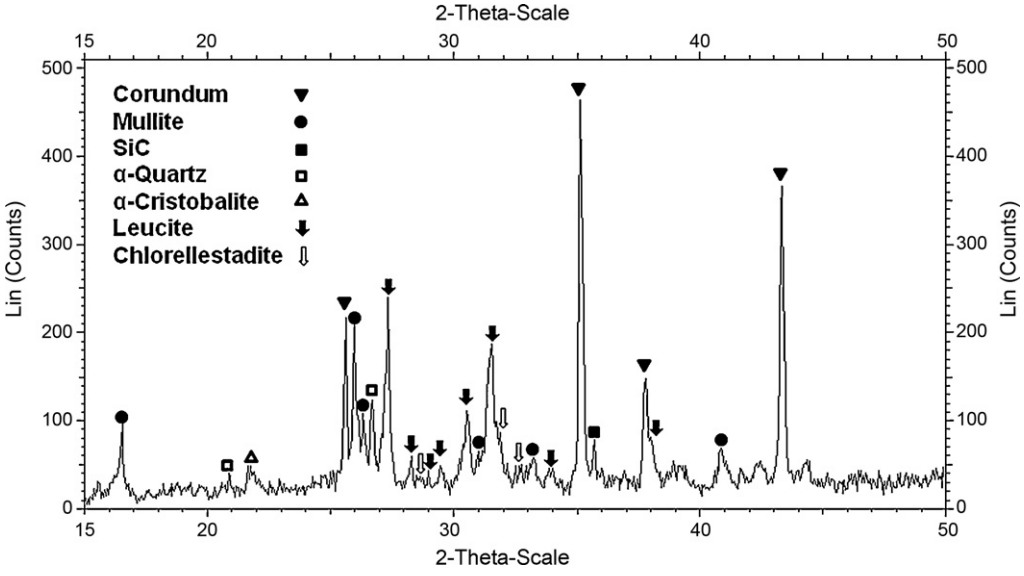

Fig. 8. X-ray diffraction of a region close to the refractory castable/build-up interface of one of the samples studied.

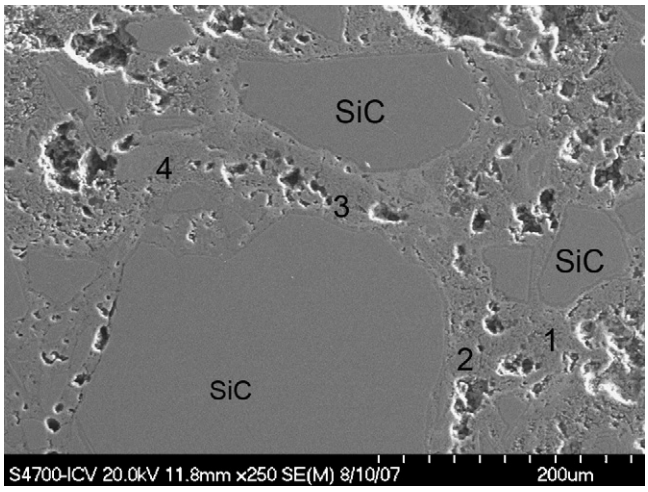

Fig. 9. SEM micrograph of a zone, close to the refractory castable/build-up interface of a high SiC concrete, showing the areas analyzed.

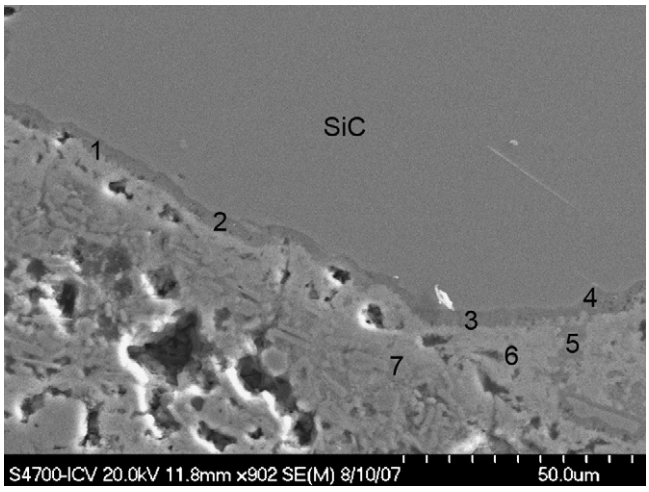

Fig. 10. SEM micrograph showing the attack of a SiC grain and areas where EDS analyses were performed.

Table 5
EDS, semi-quantitative chemical analysis of the areas marked in Fig. 9.

	Cl^-	Na_2O	Al_2O_3	SiO_2	SO_3	K_2O	CaO
pt1	0.08	0.70	21.52	20.35	11.53	34.53	11.29
pt2	0.30	1.07	19.00	32.87	5.35	32.69	9.30
pt3	0.20	0.05	21.71	26.06	7.05	30.15	14.78
pt4	0.05	0.14	11.54	21.30	10.02	30.10	12.01

Microstructural studies of polished samples of the interface refractory castables/build-up were carried out by SEM-EDS. The results have put in evidence that the main aggressive compounds (K_2O, SO_3, CaO and Cl^-) were concentrated, in all the cases, in the matrix of the refractory castables, reaching normally high values, mainly K_2O, the highest, and much less Cl^-. Fig. 9 shows a clear example of the attack of the matrix in a refractory castable with high SiC content (~45 wt.%). The semi-quantitative analysis by EDS, of the areas marked in the picture, confirms clearly, as it is shown in Table 5, the high concentration of the aggressive compounds previously mentioned.

However, the attack of the SiC grains (Fig. 10) produces around them a thin and very viscous vitreous phase, rich in silica (see Table 6), through which the diffusion of aggressive compounds is virtually nonexistent, preventing penetration and subsequent attack.

Table 6
EDS, semi-quantitative chemical analysis of the areas marked in Fig. 10.

	Cl^-	Fe_2O_3	Al_2O_3	SiO_2	SO_3	K_2O	CaO
pt1	–	–	–	99.45	–	0.55	–
pt2	0.33	0.48	–	92.59	1.69	4.92	–
pt3	–	–	2.55	91.98	–	4.32	1.15
pt4	–	–	1.99	95.05	–	2.02	0.93
pt5	0.45	–	1.98	95.70	–	1.88	–
pt6	–	–	10.86	71.15	1.96	10.53	2.49
pt7	0.32	0.05	37.17	24.60	–	35.34	–

4. Conclusions

From the results obtained, the following conclusions can be established:

Build-up: These, as it has been indicated, differ widely in composition and consequently in their mineralogy, depending on the use and the proportion of fuels employed, which essentially agrees with previous published results.[10] Normally they are formed by alternate layers of slightly different compositions as a consequence of changes in operating conditions of the furnaces. Their compactness is due to the formation of a liquid phase produced at very low temperature (~605 °C) by the action chiefly of the sylvite ($K_{1-x}Na_xCl$) and the calcium sulphate ($CaSO_4$). The origins of the main constituents of build-up are: sulphur, coming from the use of petroleum coke and tires; alkaline, mainly potassium, coming from the raw materials and agricultural and forest residues and chlorine coming mainly from plastics and meat meals. Finally, CaO is coming from the hot material in the preheater unit.

Monolithic refractories: The attack takes place due to the action of the potassium, sulphur, lime and chlorine. These mainly react with the refractory castable matrix giving rise to the formation of a vitreous phase at very low temperatures (≤985 °C) and different crystalline phases, such as those previously mentioned. The vitreous phase brings about the adherence of the rings to the refractory castables. On the other hand, most of the crystalline phases, mainly feldspar types, give rise to a volume expansion, which increases the permeability of the refractory castables and their weakness. Additionally, the depth of the attack through the matrix depends on the SiC content in the refractory castables. Consequently, as the SiC content increases the depth of attack decreases, especially if most of SiC is located in the matrix. This is because the attack of the SiC grains creates a very viscous vitreous phase, rich in silica, around the grains, through which the diffusion of corrosive agents is practically nonexistent.

Finally, note that when the build-up is removed part of the refractory material adhered to them is also removed. The thickness of the extracted material depends on the depth of the attack.

Consequently, it is essential to install a material as dense as possible with a matrix that produces a highly viscous vitreous phase when attacked by the corrosive agents, thus avoiding its penetration into the refractory castable.

References

1. Bhatty JI, Miller FM, Kosmatka SH, editors. *Innovations in Portland*. Skokie, Illinois, USA: Cement Manufacturing, CD400, Portland Cement Association; 2004, 1387 p.
2. Ishikawa Y, Hanai K, Mizuno Y, Yajima K. Monolithic refractories for the cement industry. *Taikabutsu Overseas* 1999;**19**(3):58–60.
3. Leupold H, Santowsky K, Wieland K. Improvement of resistance to alkali attack of refractory materials of the SiO_2–Al_2O_3 system for temperatures up to 1300 °C in rotary cement kilns. In: *Interceram*. 1984, special issue 29–32.
4. Ishikawa M. Monolithic refractories containing SiC. *Taikabutsu Overseas* 1995;**15**(4):26–33.
5. Mokrzycki E, Uliasz-Bochenczyk A. Alternative fuels for the cement industry. *Appl Energy* 2003;**74**:95–100.
6. Haley CAC, Chatterton MH. Solid wastes as a fuel in the cement industry in the UK. *Energy Prog* 1985;**5**(2):84–8.
7. Tamaos FD, Paotkai-Horvaoth M. Use of wastes as fuels in the cement industry: Pros & Cons. *Adv Cement Concr* 1994:82–102.
8. The European Cement Association (CEMBUREAU). Alternative fuels in cement manufacture. Technical and environmental review. Copyright: CEMBUREAU. N° Editeur: D/1997/5457/April. Rue d'Arlon 55, B-1040 Brussels.
9. Boberg LM. Alternative fuels in cement production. PhD Project 2007, Book Partner, Nørhaven Digital Copenhagen, Denmark. ISBN:978-87-91435-49-8.
10. Kurdowski W, Sobon M. Mineral composition of build-up in cement kiln preheater. *J Therm Anal Calorim* 1999;**55**(3):1021–9.
11. Stanislav Ch, Marvin JW. Ring formation process in rotary cement kilns. *ZKG, Zement-Kalk-Gips, Edition A* 1981;**34**(N-9):453–7.
12. Grosse-Daldrup H, Scheubel B. Alternative fuels and their impact on refractory linings. *World Cement* 1996;**27**(3):94–8.
13. McCaffrey R. The use of alternative fuels in the cement industry. *Refractories Worldforum* 2010;**2**(1):62–4.
14. Rouse RC, Dunn PJ. A contribution to the crystal chemistry of ellestadite and the silicate sulphate apatites. *Am Mineral* 1982;**67**:90–6.
15. Triviño Vazquez F. Identification of the incrustation in heat-recovery cyclones of the Dopol Kiln. *Materiales de Construcción (Madrid)* 1979;**176**:93–101.
16. Saint-Jean SJ, Jøns E, Lundgaard N, Hansen S. Chlorellestadite in the preheater system of cement kilns as an indicator of HCl formation. *Cement Concr Res* 2005;**35**:431–7.
17. Saint-Jean SJ, Hansen S. Nonstoichiometry in chlorellestadite. *Solid State Sci* 2005;**7**:97–102.
18. Goswami G, Padhy BP, Panda JD. Thermal analysis of spurrite from a rotary cement kiln. *J Therm Anal* 1989;**35**:1129–36.
19. Kloprogge JT, Ding Z, Martens WN, Schuiling RD, Duong LV, Frost RL. Thermal decomposition of syngenite, $K_2Ca(SO_4)_2{\cdot}H_2O$. *Thermochim Acta* 2004;**417**:143–55.
20. Irran E, Tillmanns E, Hentschel G. Ternesite, $Ca_5(SiO_4)_2SO_4$, a new mineral from the Ettringer Bellerberg/Eifel, Germany. *Mineral Petrol* 1997;**60**:121–32.
21. Rowe JJ, Morey GW, Zen CZ. System $(NaCl)_2$–$(KCl)_2$–$CaSO_4$. Geol. Surv., Prof. Pap. (US), 1972, No. 741, 37 pp. Fig. 6070 in Phase Diagram for Ceramists. Vol. V, Edited by The Am. Ceram. Soc. Inc, 1983.